Assessing the mechanical stresses of dynamic cables for floating offshore wind applications

Assessing the mechanical stresses of dynamic cables for floating offshore wind applications

D G Young[1], C Ng[1], S Oterkus[2], Q Li[3] and L Johanning[4]

[1] Offshore Renewable Energy Catapult, Blyth, UK
[2] University of Strathclyde, Naval Architecture, Ocean and Marine Engineering Glasgow, UK
[3] University of Edinburgh, School of Engineering, Edinburgh, UK
[4] University of Exeter, Offshore Renewable Energy , Exeter, UK

E-mail: david.young@ore.catapult.org.uk

Abstract. Offshore wind farms are progressing further offshore and into deeper waters, presenting the need for new substructures, including floating offshore wind turbines. These floating turbines will require dynamic cables to run through the water column, exposing them to the dynamic loadings of the marine environment. This paper presents a tool which models the stresses across a dynamic cable cross section's insulation layers when attached to a floating wind platform. Differing wave, wind and current flow conditions are applied and their impact on the stress distributions of the dynamic cable's insulation layers are presented. Finally from these stress histories, accumulated fatigue damage of the insulation is calculated and presented. The outcome of this can be used to estimate fatigue damage of a cable components cross section at any point along the cable length, and aid in cable installation configuration decisions.

1. Introduction

Offshore wind farms are progressing to having larger turbines installed as a cost effective means to reduce the cost of energy. These larger wind farms are moving further from shore and into deeper water depths. This move is presenting the need for new substructures including floating platforms for offshore turbines. Floating platform wind turbines are envisioned to be installed in water depths ranging from 50m to 200m, with the Carbon Trust estimating up to 90MW of floating wind farms are to be installed in UK waters by the end of 2018 [1].

Floating platforms will introduce new challenges for the umbilical, or array, cables that hang from the base of the platform to the seabed. This cable installation arrangement will expose the cables to the dynamic forces of the environment they would be installed in, including the actions of the waves, current flows and movement of the platform itself in response to wind/turbine interactions. Cables exposed to dynamic environmental loadings will experience dynamic mechanical stresses across their cross sections and along their length. This is a new operating consideration as traditional fixed bottom platforms have allowed cables to operate statically.

The causes of cable failures during normal operation, and excluding third party interference, can be approximately grouped into mechanical damage, water ingress and overheating which all lead to electrical failure or breakdown of the insulation layers [2]. A renewable energy insurance provider [3] highlights that most cable failure claims are related to incorrect installation, incorrect operation or electrical faults. As dynamic cables will be exposed to dynamic environments and the corresponding

force loadings, they are at higher risk of cable failure with more expected to fail during normal service lifetime.

The impact of dynamic loadings on the fatigue characteristics of dynamic cables has been investigated by [4], [5], [6] while mechanical fatigue due to environmental loadings is shown to be a concern as a propagating mechanism for water treeing in the cables insulation layers [7], [8]. The impact of differing cable bending and axial stiffness on cable fatigue damage was investigated by [9]. The axial and bending stiffness of a cable affects the cables motions in response to the dynamic environment, where having a larger stiffness reduces the cable motion. The inter-wire friction between helically wound armouring layers is found to be a determining factor in cable bending stiffness [10] while [11] investigated the impact of armouring radius reduction effects on cable axial stiffness when under tension. Similar findings are reported in [12] when comparing calculated cable axial stiffness which account for radius reduction or not.

This paper presents an assessment of the marine environment at a chosen site and presents a model which determines how the mechanical stresses across the cable cross section distribute when installed in this environment. A fatigue assessment of the cable insulation layers is completed and conclusions are drawn from the accumulated damage in differing dynamic environment loadings.

The approach presented begins with an assessment of the environment to determine the wave, wind and current loadings on the cable as detailed in section 2. An introduction to the software used and the created model is given in section 3. Section 4 provides details on how the damage is determined from the created model. Results from the model and calculated damage are presented in section 5, while section 6 gives a discussion of these results. Section 7 draws conclusions from the work, and finally section 8 highlights ongoing work.

2. Environmental Loading Assessment

Wave and current flow data from sites off the north east coast of England, as shown in Figure 1, was obtained and analysed. Wave data was obtained from a wave buoy placed at a site in 90m water depth, while current data was obtained from a 56m water depth site by an acoustic wave and current profiler, AWAC. Wind speed data correlated to wave height was obtained from two locations based in the central North Sea from the NEXT study, an extension of the North European Storm Study, NESS [13]. Briefly, NESS was initiated to produce a hind cast database of winds, waves and currents for the North European continental shelf.

Figure 1. Locations of the AWAC, 1, the wave buoy, 2, and the NEXT model locations, 3 and 4.

The locations of the wave buoy, AWAC and NEXT study sites were determined to be within the same coarse grid of the central North Sea. Therefore it was assumed the environment exhibited at each site would be similar, meaning the wave environmental data captured at the wave buoy site would be the same wave data that would be captured at the AWAC site or the NEXT sites, and vice versa. The water depths at the sites were differing, so the captured current flow speed data was fitted to the power law velocity profile using equation 1 [14] , assuming a shear profile due to seabed roughness. This was then extrapolated, allowing for current velocity calculations at other water depths:

$$\frac{U_z}{U_{max}} = (\frac{Z}{H})^{1/n} \quad (1)$$

Where U_z is the water velocity in ms^{-1} at point Z, U_{max} is the maximum water velocity in ms^{-1}. Z is the vertical position from the seabed in m, H is the full tidal depth in m and n is the power law coefficient.

To use wind data near the wave data site it was necessary to assume that the wind generated the waves and thus the wave height was directly related to the wind speed. The NEXT data sites present wave height binned with a corresponding wind speed 10m above sea level. This data was used to create a best fit curve that could be used to back calculate a corresponding wind speed for the wave heights recorded by the wave buoy. For this reason it was also assumed that the wind and waves were coming from the same general directions.

This model includes a tension legged floating wind platform incorporating the NREL 5MW turbine. This turbine has a hub height of 90m, therefore by using the equations laid out in the guidelines for the certification of offshore wind turbines [15] the wind speed at the hub height was calculated using:

$$V_z = V_{hub}(\frac{h}{h_{hub}})^{\propto} \quad (2)$$

Where V_z is the wind speed at height h in ms^{-1}, h is the height about still water line in m, h_{hub} is the hub height above still water line in m, and α is the power law exponent, [15] assumes that α is equal to 0.14 for all wind speeds.

3. Dynamic Cable Model

To understand the stresses that the loading environment would impose upon a dynamic cables cross section, the whole floating platform system needs to be analysed initially as a global model. The output from the global model can then be used to simulate the stress distributions and time history for a local mechanical model of the cable cross section.

Details of this model can be found in [16] however for clarity a condensed version of the essentials will be provided here.

3.1. Global Dynamic Model

This model was created using the proprietary marine dynamics software OrcaFlex by Orcina. OrcaFlex was used to estimate the loadings on the dynamic cables installation length in response to the actions of the waves, currents, wind and the movements of the floating platform itself. For this work the cable was split into 0.5m lengths and the software employs a lumped mass approach to solve the cables dynamic behaviour.

Required inputs for the dynamic model include the environmental loadings and properties of the cable, including its geometry, length, axial and bending stiffness's.

The MIT/NREL reference 5MW tension leg platform [17] is included in this work and its movements modelled. This is a platform of 18m waterline depth and almost 50m draft. It has four 27m long pontoons, each having two mooring lines attached to its end. Fastlink is a FAST-OrcaFlex interface package that couples the software OrcaFlex with FAST. The hydrodynamics of the cable are modelled

using OrcaFlex. The NREL 5MW reference turbine, tower, floating platform and structural dynamics, aerodynamics control and electrical drive dynamics are modelled using FAST. This allows for the coupling of the effects of the wind on the turbine with the effects of the waves and currents on the platform.

3.1.1. Dynamic Cable. The cable modelled for this work is based on 280m length of a JDR dynamic cable [18] used in previous oil and gas applications. Figure 1 gives some of the cables mechanical parameters. The cable axial stiffness was calculated using works laid out in [11], and the bending stiffness using [10].

Table 1. Mechanical Parameter of the Dynamic Cable.

Mechanical Properties	
Outer Diameter	154mm
Outer Sheath Material	Extruded Polyethylene
Cable Armouring	Galvanised Steel Wire
Minimum Bend Radius	2000mm
Safe Working Load	250kN
Diameter to Weight Ratio	4.27m^2/Te

3.2. Mechanical Model
The mechanical model is used to determine the stress time histories and distributions across the cables cross section. This local model uses the outputs of the global dynamic model to allow the user to determine the stresses acting on individual cable components, highlighting areas of greatest mechanical stress. Plane and shear stresses are calculated for each of the cables six degrees of freedom as well as combined into a von Misses stress.

3.2.1. Finite Element Analysis. A finite element analysis, FEA, of the cable cross section was constructed using ANSYS Mechanical software. This proved an effective method to determine the interactions between different components of the dynamic cables cross section. Similar works on dynamic umbilical cables [19], [20] both used an alternative FEA software called UFlex2D. This is a custom built software for umbilical cross sections however ANSYS was used here for its coupling abilities with OrcaFlex.

3.3. Model Assumptions
To balance accuracy and computational expense some assumptions were made during this analysis. The cable stiffness was assumed to come from the cable armouring layers. The armouring layers were simplified to thin walled cylinders for the mechanical model, similar to [9]. This assumption follows the thought that the armouring layers are always in stick mode rather than slip mode so that individual armouring wires do not slide over one another during operation. The cable component materials were assumed to be linear elastic and that they were glued together in the FEA, meaning they could not penetrate another components surface.

4. Fatigue Damage Calculations
An output from the mechanical model are the stress histories of the components of the dynamic cables cross section. A stress based approach to fatigue was used as the stresses exerted upon the cross section are lower than the design yield stresses of the cable component materials.

Accumulated fatigue damage of the dynamic cable insulation layers are calculated using the Palmgren-Miner linear damage rule, equation 3, and the corresponding S-N curve for that material.

$$D = \sum_{i=1}^{k} \frac{n_i}{N_i} \tag{3}$$

Where for k different stress levels and the average number of cycles to failure at the ith stress, S_i, is N_i and n_i is the number of cycles are accumulated stress S_i. No fatigue limits were set for this initial work as compression and tension are both assumed to contribute to fatigue. The S-N curve used for the XLPE insulation layers was obtained from [8].

5. Results

5.1. Environmental loading Assessment

Using the data from [13] the relationship between the significant wave height and the wind speed is plotted in Figure 2. This plot allows for the determining of the wind speed for the wave heights recorded by the buoy. Figure 3 shows a binned scatter plot of the significant heights and zero crossing period of the waves recorded by the buoy.

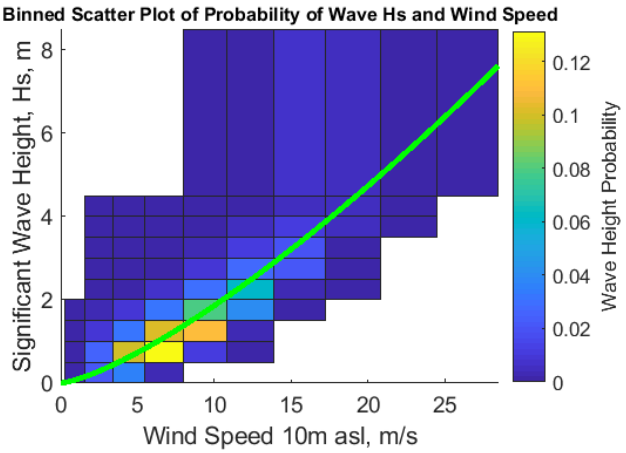

Figure 2. Relationship of wave height to wind speed.

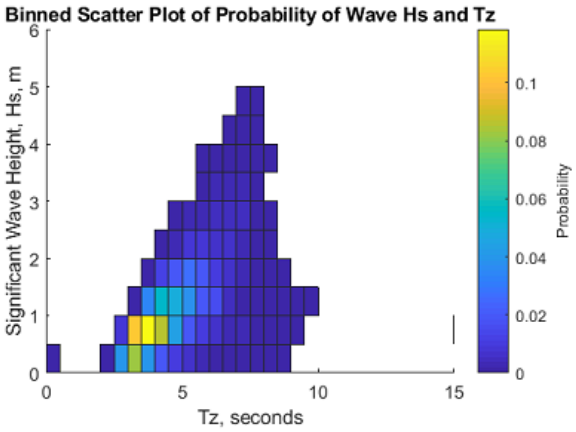

Figure 3. Binned scatter plot of significant wave height and zero crossing period.

Using the recorded wave heights from Figure 3, and equation (2), the wind speeds the turbine is exposed to are presented in table 2.

Table 2. Corresponding wave heights and wind speed.

Significant Wave Height(m)	Wind Speed 10m asl (ms^{-1})
0.25	2.2
0.75	5.1
1.25	7.4
1.75	9.5
2.25	11.5
2.75	13.4
3.25	15.1
3.75	16.8
4.25	18.5
4.75	20.1

From these results, the largest wind speed the turbine would face 10m asl is 20.1ms^{-1}, roughly corresponding to gale force winds and a Beaufort Force of 8 on the Beaufort scale.

The wave directions were also recorded by the wave buoy and are presented in a wave direction rose shown in Figure 4. As the NESS model sites did not provide much information to back calculate the wind directions, the winds and waves are assumed to come from the same direction for this work.

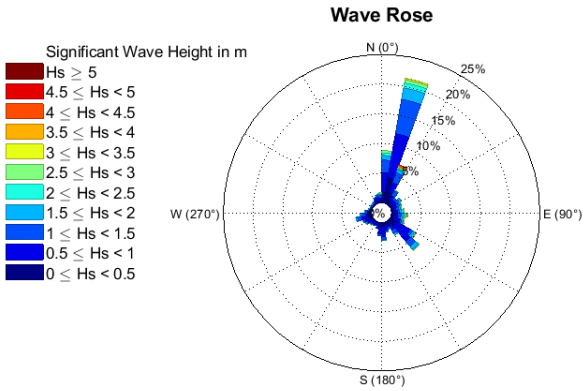

Figure 4. Wave rose of wave directions and height

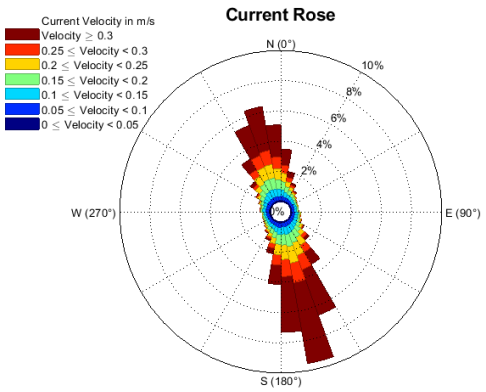

Figure 5. Current rose of current direction and speed

From figure 4 it can be seen that the wave direction is predominantly from the North, so for the model the waves and therefore wind are assumed to be coming from one direction only.

The data recorded by the AWAC was used to determine the current magnitude and direction and is presented in Figure 5. From this it can be seen that the current direction is approximately bi-directional, traversing up and down the North East of England coastline. The average current speed for each recorded water depth was calculated and extrapolated to a 200m water depth with the curve plotted in Figure 6. This curve was compared to the theoretical current profile calculated using equation (1).

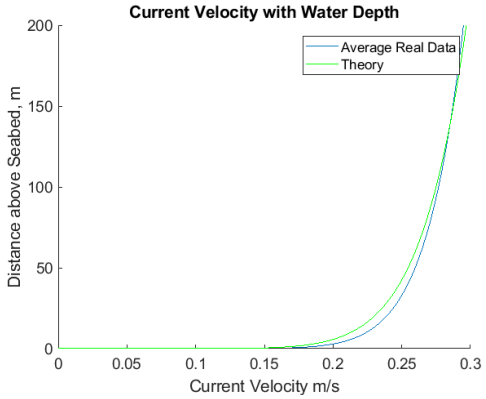

Figure 6. Current velocity profile with water depth

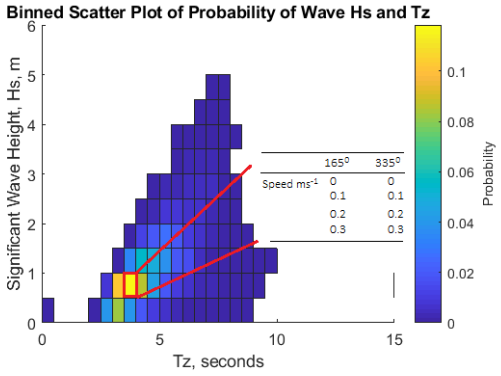

Figure 7. Subdivisions of wave loadings by current speed and direction

Figure 7 illustrates how each wave loading scenario was subdivided by current speed and directions. This plot was generated based on the assumption that the current flow is bi-directional and accelerates and decelerates from 0.3ms^{-1} in one direction to 0.3ms^{-1} in the other, similar to results found in [21]. From the calculated results the following environmental loading conditions were used for the model.

Table 3. Environmental Loadings

Environmental Loadings	
Wave height (m)	0.25 – 4.75
Wave period (s)	0.25 – 9.75
Wave direction (^{0})	15
Wind Speed (ms^{-1})	2.2 – 20.1
Wind Direction (^{0})	15
Current Speed ms^{-1}	0-0.3
Current Direction (^{0})	165 and 335

5.2. Dynamic Cable Model Output

Similar to works presented in [16] and [4], the hang off point of the cable is an area of concern for fatigue. Further investigation of the stress distributions and accumulated damage at this point specifically shall be given in these works, however it should be noted that any point along the length of the cable can be chosen.

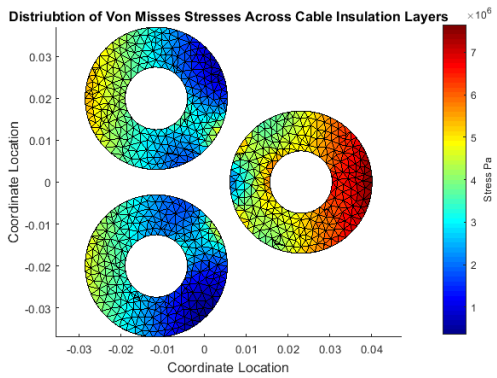

Figure 8. Stress distributions at hang off point.

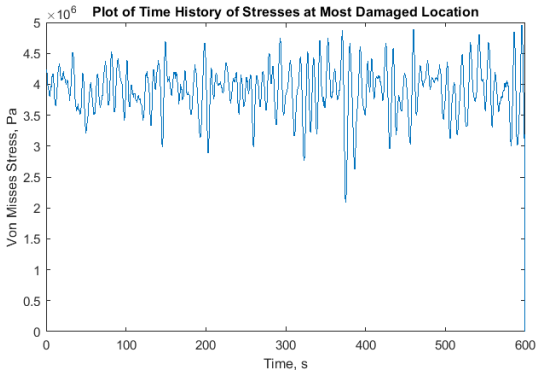

Figure 9. Stress time history at most damaged location.

Figure 8 shows the von Misses stress distributions of the cross linked polyethylene, XLPE, insulation layers at the cable hang off point. While any component of the cable cross section can be investigated, the XLPE layer shall be looked at specifically for further analysis. The stresses of the insulation layers are investigated due to concerns of water tree growth. It should be noted that for any cable component the plane or shear stresses can be deduced. Figure 8 is plotted using the outputs of the global dynamic model including, effective tension, x-bend moment, y-bend moment etc. and coupling them with the local mechanical model.

From the distribution, the stress time history of each location can be extracted. Figure 9 shows the stress time history of the XLPE location that experienced the most damage. It should be noted that the first 30 seconds of each simulation was discarded to allow for environment ramp up avoid the large stress amplitudes due to the platform moving from an initial stationary position.

5.3. Fatigue Damage

For each location the time history can be extracted, and the accumulated fatigue damage can be calculated using equation (3). This allows for the distribution of fatigue damage across the cable insulation layers to be plotted, shown in figure 10.

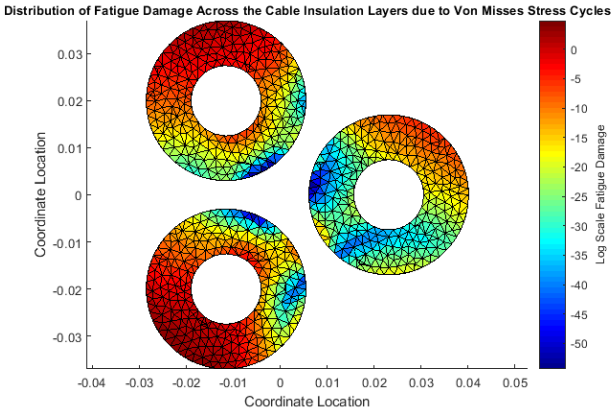

Figure 10. Log scale distribution of fatigue damage.

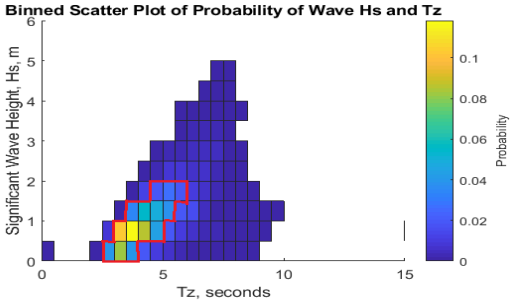

Figure 11. Wave spectrum distribution with greatest probability conditions highlighted.

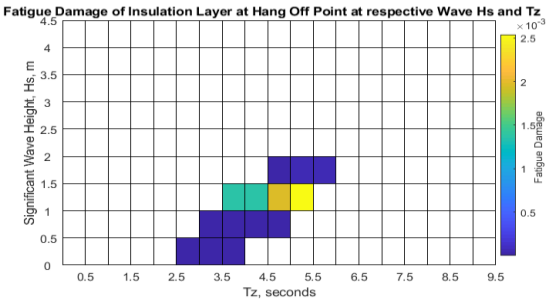

Figure 12. Calculated fatigue damage for the highlighted wave spectrum conditions.

Figure 11 shows the previously calculated wave spectrum, but with the most frequently occurring waves circled. Figure 12 shows the damage calculated for each of these wave conditions. It should be noted that these total damages incorporate the damages calculated for each of the current velocities and directions as depicted in Figure 7, but does not account for the occurrence of each wave type.

6. Discussion

The presented work can be used to give an estimation of the fatigue damage of any component of a dynamic cable's cross section. This work focused on the von Misses stress distribution, σ_{vm}, of the dynamic cable's insulation layers and assumed that in these preliminary works that both compression and tension contributed to damage within the cable insulation layers. Work was completed to deduce the impact of varying wave heights, periods and current velocities on the mechanical fatigue damage of the insulation layers of a dynamic cable. It was found that greater wave heights resulted in a greater level of fatigue damage. This could be contributed to greater wave heights causing a greater heave of the floating platform, therefore increasing the tension on the dynamic cable.

It was found that a longer wave period increases the fatigue damage calculated. This is contrary to the thought that a greater wave frequency would inhibit the platform from returning to its undisturbed position, keeping the cable in a state of stress. While wave celerity does increase with wave period, the orbital, or horizontal velocities, of the water particles decrease with wave period. These velocities can determine the force of the impact of the waves on the floating platform using Morrison's equation, where the force in the x-direction on a body in unsteady flow with velocity *U(t)* is:

$$F_x(t) = \rho C_m V \dot{U} + \frac{1}{2}\rho C_d A\,|U|U \tag{4}$$

Where V is the body volume in m^3, ρ is the mass density of the fluid in kgm^{-3}, $\dot{U}$ is the flow acceleration in ms^{-2}, A is the body reference area in m^2, C_d and C_m are the drag and momentum coefficients respectively.

Using equation 4, it can be quickly deduced that a reduction in velocity would result in a reduced force exerted on the platform from the waves, thus reducing the displacement of the platform. From figure 12 the wave periods ranging from 3.75s to 5.25s were investigated to determine the displacements of the floating platform, shown in table 4.

Table 4. Displacement of floating platform at varying wave period and wave height 1.25m

Wave Period Tz (s)	Average X displacement (m)	Average Y displacement (m)	Average Z displacement (m)	Damage
3.75	3.34	-0.081	-0.037	0.0013
4.25	3.34	-0.080	-0.037	0.0013
4.75	3.35	-0.080	-0.037	0.0019
5.25	3.34	-0.08	-0.037	0.0024

From table 4 it is seen that at varying wave periods the average platform displacement minimally changed, if at all, however the damage of the dynamic cable insulation layers increased. This increase in damage can perhaps be explained by a greater frequency of platform movement. If a closer look is taken at the stress time histories of the most damaged insulation locations, it can be seen that a wave period of 5.25s compared to a period of 3.75s, produces a stress history with more stress amplitudes, evident in the jagged plot for the 5.25s wave period shown in figure 13. This greater stress frequency can perhaps be due to the period of the waves matching the eigen period of the system, however this has not been investigated in any detail.

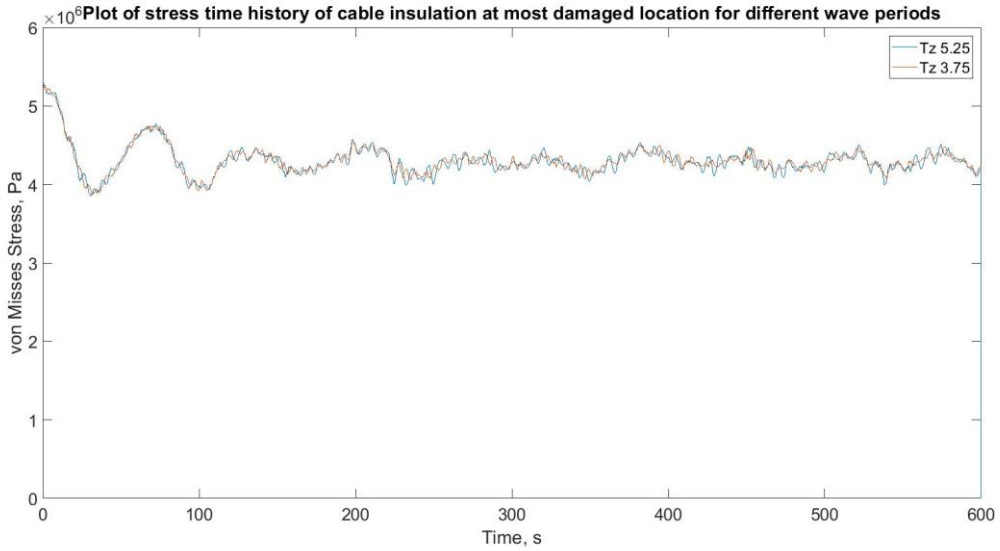

Figure 13. Stress time histories of the cable insulation at differing wave periods

It is important to note that the magnitude of the fatigue damage of the insulation layers is small. This is to be expected as the armouring layers surrounding the insulation layers are protecting them from damage. However when the extreme cases were simulated for a H_s of 4.75m and a Tz of 7.75s, the fatigue damage calculated was much larger than 1, indicating a cable failure, even of the insulation layers. Unfortunately this result was omitted from figure twelve due to its fatigue value being much larger than the others. As figure 12 shows the fatigue damages scaled to one another, this distorts the plot and results in the details of the smaller fatigue differences being lost. Furthermore as this work is the initial steps in analysing water treeing within the insulation layers, extreme wave conditions would cause a cable failure outside of that of water treeing.

When considering the impact of varying current speeds and directions it was found that when the current is travelling up the coast in Figure 1 (direction 165^0) the damage is greater than when it is travelling in the opposite direction, 335^0. It can be seen that when the current speeds are at their greatest in the tidal cycle, this also corresponds to a greater level of cable insulation fatigue damage. This output from the model could be used in the future to aid in cable installation layout and orientation decisions to reduce cable fatigue.

While this work presented von Misses stress distributions, the model allows the user to look at individual plane or shear stresses a component experiences. When these individual stresses are looked at for a particular environmental loading, it can be see that the largest contributing stress is σ_{zz} as seen in table 5.

Table 5. Magnitude of insulation fatigue damage at most damaged insulation location due to corresponding stress type.

Stress Type	Fatigue Damage
σ_{xx}	4.53e-41
σ_{yy}	5.28e-50
σ_{zz}	5.15e-06
σ_{xy}	2.74e-46
σ_{yz}	4.65e-25
σ_{xz}	3.41e-30
σ_{vm}	9.00e-06

In this case, this highlights that it is cable bending that contributes to insulation fatigue at the hang off point, rather than cable tension.

Unless in extreme storm conditions, the fatigue damage of the cable insulation calculated was very small. This could be a weakness in the model being under conservative. However it is important to note that the cable modelled was a dynamic cable used in historic oil and gas applications, and would have a much larger cable axial and bending stiffness than one that would be used for floating offshore wind applications. A further weakness of the model is that for the fatigue damage on the insulation layers, only one S-N curve could be found in previous works. To give a greater credibility to the results a larger number of S-N curves would have been desirable.

7. Conclusions

This work presents a method to determine mechanical fatigue damage across a dynamic cable's cross section, specifically the insulation layers, when exposed to a dynamic marine environment. It can be used as a tool to compare the insulation fatigue damage at differing lengths along the cables length. Individual components of the cable cross section can be investigated, giving way to a more comprehensive fatigue assessment of dynamic cables.

It was found that increasing wave height increases cable insulation fatigue damage in deep water applications. Increasing current velocities also increases cable insulation fatigue damage. Current direction plays a role in cable insulation fatigue damage, aiding in installation arrangement decisions. Finally, the works suggests that it is the stresses due to cable bending, as opposed to tension that contribute most to a dynamic cable's insulation fatigue damage.

8. Future Work

The next stages of this work is to use the most damaged cable insulation locations as initiation points of insulation water treeing. Using the stress cycles calculated within these works is hoped to allow for the modelling of cracks within the insulation as propagating mechanisms of water treeing.

The electrical stresses across the insulation layers are then to be modelled. It is envisioned this work serves at the first step in the development of a coupled mechanical and electrical fatigue model of the cable insulation which considers both mechanical stresses and electrical stresses due to the cable being energized.

9. Acknowledgements

The authors would like to thank the Energy Technology Institute and the Research Council Energy Programme for funding this research as part of the IDCORE programme (grant EP/J500847), and the Offshore Renewable Energy Catapult for providing technical assistance and equipment. A special thanks to Orcina for providing OrcaFlex software and to JDR cables for allowing presentation of cable data.

References

1. Carbon Trust. Floating Wind Joint Industry Project: Policy & Regulatory Appraisal [Internet]. 2017 [cited 2018 Mar 14]. Available from: https://www.carbontrust.com/resources/reports/technology/floating-wind-policy/

2. Marazzato H, Barber K, Jansen M, Graeme B. Cable Condition Monitoring to Improve Reliability. Olex Australia; 2004.

3. GCube. Down to the Wire: An Insurance Buyer's Guide to Subsea Cabling Incidents, June 2016 Report. GCube Insurance Services; 2016.

4. Thies PR, Johanning L, Smith GH. Assessing mechanical loading regimes and fatigue life of marine power cables in marine energy applications. Proc Inst Mech Eng Part O J Risk Reliab. 2011 Oct;1748006X11413533.

5. Buitrago J, Swearingen SF, Ahmad S, Popelar CF. Fatigue, Creep and Electrical Performance of Subsea Power Cable. In American Society of Mechanical Engineers; 2013 [cited 2018 May 23]. p. V003T03A028-V003T03A028. Available from: http://proceedings.asmedigitalcollection.asme.org/proceeding.aspx?articleid=1786236

6. Thies PR, Johanning L, Dobral C. Parametric Sensitivity Study of Submarine Power Cable Design for Marine Renewable Energy Applications. 2017 Jun 25;V03BT02A010.

7. Ildstad E, Bardsen H, Faremo H, Knutsen B. Influence of mechanical stress and frequency on water treeing in XLPE cable insulation. In: , Conference Record of the 1990 IEEE International Symposium on Electrical Insulation, 1990. 1990. p. 165–8.

8. Wang Z, Marcolongo P, Lemberg JA, Panganiban B, Evans JW, Ritchie RO, et al. Mechanical fatigue as a mechanism of water tree propagation in TR-XLPE. IEEE Trans Dielectr Electr Insul. 2012 Feb;19(1):321–30.

9. Yang S-H, Ringsberg JW, Johnson E. Parametric study of the dynamic motions and mechanical characteristics of power cables for wave energy converters. J Mar Sci Technol. 2017;

10. M. Raoof, Davies TJ. Determination of the bending stiffness for a spiral strand. J Strain Anal Eng Des. 2004;39(1).

11. Chen X, Fu S, Song L, Zhong Q, Huang X. Stress analysis model for un-bonded umbilical cables. Ocean Syst Eng. 2013;3(2):97–122.

12. Ekeberg KI, Ottesen T, Aarstein J, Saevik S, Ye N, Igland R. Predicting, Measuring and Implementing Friction and Bending Stresses in Dynamic Umbilical Design. In Offshore Technology Conference; 2006 [cited 2018 Mar 15]. Available from: https://www.onepetro.org/conference-paper/OTC-17986-MS

13. Fugro GEOS, Health & Safety Executive. Offshore Technology Report, "Wind and wave frequency distributions for sites around the British Isles." 2001.

14. Lewis M, Neill SP, Robins P, Hashemi MR, Ward S. Characteristics of the velocity profile at tidal-stream energy sites. Renew Energy. 2017 Dec 1;114:258–72.

15. Germanischer Lloyd Rules and Guidelines, Industrial Services. Guideline for the Certification of Wind Turbines,. 2005.

16. Young D, Ng C, Oterkus S, Li Q, Johanning L. Predicting failure of dynamic cables for floating offshore wind. In: 3rd International Conference on Renewable Energies Offshore. 2018.

17. Jonkman B. FAST-OrcaFlex Interface | NWTC Information Portal [Internet]. 2016 [cited 2018 Mar 15]. Available from: https://nwtc.nrel.gov/OrcaFlexInterface

18. Featherstone J. Dynamic Subsea Power Cables for Floating Wind & 66kV Subsea Power Cables, 6th Annual Advanced Submarine Power Cable & Interconnection Forum, Berlin. 2017 Jun.

19. Silva D, Balena R, Lisbôa R. Methodology for Thermoplastic Umbilical Cross Section Analysis. 2012 Jul 1;407–11.

20. Gaidai O, Ye N, Jin J, Reid D, Mainçon P. Fatigue Analysis Methods of Dynamic Umbilicals. In International Society of Offshore and Polar Engineers; 2015 [cited 2018 May 15]. Available from: https://www.onepetro.org/conference-paper/ISOPE-I-15-595

21. Pheonix A. Development of a tidal flow for optimisation of tidal turbine arrays. Access to Research at NUI Galway; 2018.